Journal of Applied Electrochemistry **34**: 427–438, 2004.

The role of the WO_x ad-component to Pt and PtRu catalysts in the electrochemical CH_3OH oxidation reaction

L.X. YANG, C. BOCK*, B. MacDOUGALL and J. PARK
National Research Council Canada, Montreal Road, Ottawa, Ontario K1A OR6, Canada
*(*author for correspondence, fax: 613 941 2529, e-mail: Christina.Bock@nrc.ca)*

Received 15 May 2003; accepted in revised form 6 November 2003

Key words: fuel cells, methanol oxidation, tungsten oxide

Abstract

High surface area carbon-supported platinum-based catalysts, Pt/C, $PtWO_x$/C, PtRu/C and $PtRuWO_x$/C, were prepared via a chemical reduction route using single metal precursor salts. The catalyst particles were found to be in the nanoscale range, and the addition of Ru clearly decreased the particle size. The Ru was found to be partially incorporated into the face centered cubic lattice of Pt and to form a single Ru catalyst component. X-ray diffraction and X-ray photon spectroscopy did not provide evidence for electronic interactions between WO_x and Pt as well as WO_x and Ru. However, the addition of tungsten to the $PtRuWO_x$/C catalyst resulted in a high degree of catalyst particle agglomeration. Both Ru containing catalysts showed significantly higher activities for the CH_3OH oxidation reaction in terms of Pt + Ru mass as well as electroactive Pt + Ru surface area than the Pt/C and $PtWO_x$/C catalysts. The addition of tungsten appeared to mainly result in some 'physical' modification of the catalytically active Pt and Ru surface components such as differences in electroactive surface area rather than promotion of the CH_3OH oxidation reaction via a true catalytic mechanism.

1. Introduction

Direct methanol fuel cells (DMFCs) have received much attention due to their promising use as low temperature power sources [1, 2]. A major challenge for the successful implementation of DMFCs is the improvement of the Pt based anode catalysts towards the CH_3OH oxidation reaction. It is well known that the addition of Ru to Pt based catalysts lowers the overpotential for the methanol oxidation reaction significantly through a so called bifunctional mechanism [3, 4] that can be summarized as follows:

$$Pt + CH_3OH = PtCO_{ads} + 4H^+ + 4e^- \quad (1)$$

$$Ru + H_2O \rightarrow Ru(OH)_{ads} + H^+ + e^- \quad (2)$$

$$PtCO_{ads} + Ru(OH)_{ads} \rightarrow CO_2 + Pt + Ru + H^+ + e^- \quad (3)$$

The presence of oxide free Pt is essential for the hydrogen abstraction reaction from CH_3OH (Reaction 1). The formation of the adsorbed OH species (Reaction 2) is believed to be a critical step in the CH_3OH oxidation reaction to CO_2. This reaction takes place at low potentials for the case of Ru, and, in fact, until now PtRu catalysts have shown the most promising performance as anode catalyst for DMFCs.

Numerous attempts have been made to further improve the performance of the Pt based anode catalysts for the CH_3OH oxidation reaction using a large range of two and multi-component Pt systems such as PtSn, PtRuOsIr, $PtWO_x$ etc. [5–7]. The addition of WO_x has attracted some attention, and improved methanol oxidation activities of WO_x containing Pt based catalyst systems have been reported [7–9]. Shen et al. tested high surface area $PtWO_x$ anodes, made using an electrodeposition route, for the CH_3OH oxidation reaction [7]. They obtained reasonably high CH_3OH oxidation currents per geometrical anode area, however, the actual turnover number for the CH_3OH oxidation reaction per Pt site turned out to be small [10]. Shukla et al. prepared high surface area carbon supported $PtWO_x$ catalysts via a chemical reduction route and reported superior methanol oxidation activities per mass of Pt for $PtWO_x$ as compared to WO_x free Pt catalysts [8]. Somewhat higher CH_3OH oxidation activities per total carbon supported catalyst weight for $PtRuWO_x$ as opposed to PtRu catalysts were reported by Goetz and Wendt who tested the catalysts under real fuel cell operating conditions [9]. In the majority of these studies, CH_3OH oxidation activities for different catalysts were compared per weight of catalyst. Therefore, it appears necessary to establish whether the reported improved activities for the WO_x containing CH_3OH oxidation catalysts are due to true catalytic properties such as a bifunctional

mechanism and/or whether the addition of WO_x modifies 'physical' catalyst particle properties such as particle size, surface area and surface concentrations of the actual catalyst components.

In this work carbon supported Pt based catalysts containing WO_x and/or Ru have been prepared by chemical reduction of the corresponding precursor salts. All catalysts were characterized using X-ray diffraction (XRD), X-ray photon spectroscopy (XPS) and transmission electron microscopy (TEM). Slow sweep CO stripping voltammetry was also employed as an *in situ* probe to test the ability of the catalysts to oxidize adsorbed CO as well as a measurement of the electroactive surface area of the noble metal catalyst components. The activities of the catalysts for the CH_3OH oxidation reaction were determined at 60 °C employing slow sweep cyclic voltammetry (CV) as well as the more fuel-cell relevant potential time transients obtained galvanostatically. The CH_3OH oxidation activities for the different catalysts were compared using the more relevant CH_3OH oxidation currents normalized by the Pt + Ru mass as well as comparing true catalytic activities, that is, CH_3OH oxidation currents normalized by the total noble metal surface area.

2. Experimental details

2.1. *Catalyst preparation*

The carbon black supported Pt based catalysts were prepared using a chemical reduction method involving $NaBH_4$ (99% purity, Aldrich), as described by Shukla et al. [8]. 10 ml of the following single metal salt precursor solutions were prepared: (i) Pt/C catalyst: 0.42 g of $H_2PtCl_6 \cdot 6H_2O$ (99.9% metals basis, Alfa Aesar); (ii) $PtWO_x$/C catalyst: 0.42 g of $H_2PtCl_6 \cdot 6H_2O$ and 0.08 g of $(NH_4)_6H_2W_{12}O_{40}$ (99.9 + x%–W, Strem Chemicals); (iii) PtRu/C catalyst: 0.42 g $H_2PtCl_6 \cdot 6H_2O$ and 0.174 g $RuCl_3$ (99.9% metals basis, Alfa Aesar); and (iv) $PtRuWO_x$/C catalyst: 0.42 g $H_2PtCl_6 \cdot 6H_2O$, 0.174 g $RuCl_3$ and 0.08 g of $(NH_4)_6H_2W_{12}O_{40}$. A particular precursor salt solution was slowly added to a 80 °C suspension of 0.5 g carbon black (acetylene black, >99.9% purity, Alfa Aesar) in 20 ml H_2O. The mixture was stirred at 80 °C in a tall, open beaker for 1 h and subsequently heated in an air oven at 100 °C for 4 h, resulting in a dry and precursor salt impregnated form of the carbon powder. After cooling, the impregnated carbon powder was ground using a mortar and was transferred quantitatively to a three way round bottom flask and 20 ml of H_2O was added. The pH of the formed suspension was adjusted to 1 using H_2SO_4. 10 ml of 0.2 M $NaBH_4$ were dropwise added at 80 °C and the suspension was subsequently refluxed at 80 °C for 24 h. After cooling, the suspension was filtered, washed with H_2O and dried in an oven at 80 °C. UV/VIS spectra of the washing solutions were obtained to estimate the possible loss of catalyst components. UV/VIS calibration curves for a particular catalyst component were obtained using solutions made of the corresponding precursor salts.

This catalyst preparation procedure and amounts of precursor salts used here are equivalent to the following theoretical atomic ratios: $PtWO_x$/C catalyst: 1:0.3 Pt:W; PtRu/C catalyst: 1:1 Pt:Ru and $PtRuWO_x$/C catalyst: 1:1:0.3 Pt:Ru:WO_x and resulted in Pt and Ru loadings of 32 and 16 wt % per carbon, respectively. Furthermore, the $RuCl_3$ was dried at 130 °C prior to its use for the precursor salt solutions.

2.2. *Techniques and instrumentations*

XPS spectra were obtained using a Kratos Axis Ultra spectrometer equipped with a monochromatized AlK_α source. The catalyst powders were attached to sticky Cu tape (3M cupper tape, Soquelec, Montreal) for the XPS analyses. Deconvolutions of the XPS spectra were performed using a Grams_32 Spectral Note base software program. A Philips CM 20 TEM was also employed. For the TEM analyses, the carbon supported catalyst powders were ultrasonically suspended in H_2O and a small amount of the catalyst powder suspension was applied to a carbon film on 300 mesh Cu grid (Marivac). A Scintag XDS2000 system was employed using a CuK_α source to obtain XRD spectra of the carbon supported catalysts. The scanning angle extended from 20° to 80° with a scanning rate of 0.04°, accumulating data for 10 seconds per step. Silicon powder (typically 1 to 20 μm, 99.9985% purity, Alfa Aesar), that was homogeneously grounded with the carbon supported catalysts, was used as an internal standard. The software program Topas 2 (DIFFRAC^{PLUS} Topas, Bruker axs) was employed to extract lattice parameter constants from the experimental XRD spectra. The entire XRD spectra (20° to 80°) were employed to analyse the data. The XRD, XPS and TEM characterizations were carried out on the unused, as-prepared, catalyst powders. All electrochemical experiments were carried out using an EG&G 263 potentiostat driven by Corrware software program (Scribner). A Shimadzu UV-1201S UV/VIS spectrometer was also employed.

2.3. *Cells and electrodes*

Three-compartment cells, in which the reference electrodes were separated from the working and counter electrode compartment by a Luggin capillary, were employed for the electrochemical studies. Large surface area Pt gauzes served as counter electrodes and a mercury–mercury sulfate (MSE) electrode was used as reference electrode. The working and counter electrodes were well separated by about 2.5 cm. All potentials in this study are reported with respect to standard hydrogen electrode (RHE), the potential of the MSE being 0.68 V vs RHE [11].

The catalyst powders were formed into electrodes by sonicating 13 mg of the carbon supported catalyst powders in 1 ml of H_2O and 300 μl of Nafion® solution (5 wt %, Aldrich) for 15 min., that is, forming a catalyst ink. Subsequently, 10 μl of catalyst ink was applied to form a thin layer of about 0.5 cm^2 geometrical area on a gold foil (0.5 cm × 2 cm × 0.1 cm, Goodfellow, 99.95% metal basis). The catalyst layer was then dried at 80 °C in an air oven for 30 min. Electrical contact was made by firmly attaching a Au wire via a small hole to the Au foil. The following theoretical Pt + Ru mass (m_{Pt+Ru}) loadings per electrode were achieved in this manner: 24 μg for Pt/C, 23 μg for $PtWO_x$/C, 33 μg for PtRu/C and 31 μg for $PtRuWO_x$/C catalyst. In some cases, a polycrystalline Pt foil (0.1 mm thick, 99.99% metal basis, Alfa Aesar) was also employed as working electrode. The use of these thin layer electrodes prepared not involving higher temperature treatment and/or hot pressing minimizes changes in catalyst properties such as enhanced catalyst particle agglomeration (i.e., increase in particle size), surface segregation of Pt etc., and also ensures complete utilization of the catalyst particles for the CH_3OH oxidation reaction.

2.4. *Adsorbed CO (CO_{ads}) stripping voltammetry*

CO was adsorbed onto the Pt based electrodes at 0.08 V by bubbling CO gas (Matheson purity, Matheson gas) through the 0.5 M H_2SO_4 solution for 25 min. Solution CO was subsequently removed by bubbling Argon gas (high purity, Air products) for 35 min. holding the potential at 0.08 V. The potential was then cycled at 10 mV s^{-1} starting at 0.08 V for two complete oxidation and reduction cycles.

2.5. *Electrode conditioning prior to CO_{ads} and CH_3OH oxidation studies*

In this work the catalyst electrodes were conditioned for 30 complete oxidation/reduction cycles at 100 mV s^{-1} between 0 and 0.9 V in 0.5 M H_2SO_4 before any electrochemical oxidation studies, such as CO_{ads} and CH_3OH oxidation were carried out. The CV characteristics (change in charge reflecting the Ru electrochemistry) suggested that only a small amount of Ru (~4%) was lost from the PtRu/C and $PtRuWO_x$/C catalysts as a result of the conditioning process.

2.6. *Solutions and chemicals*

All chemicals used in this work were A.C.S. grade along with high resistivity 18 MΩ H_2O. Methanol oxidation studies were carried out in deoxygenated 0.5 M H_2SO_4 + 1 M CH_3OH solutions at 60 °C, while all other electrochemical experiments were carried out at room temperature. The volume of the solution placed in the working electrode compartment was about 50 ml.

3. Results and discussion

3.1. *Theoretical and experimental atomic ratios of the carbon supported catalysts*

Table 1 summarizes the theoretical and experimental atomic ratios of the carbon supported Pt based catalysts made and studied in this work. The experimental bulk atomic ratios were estimated from UV/VIS spectra obtained for the washing solutions of the catalysts, as described in the experimental section, while the theoretical bulk atomic ratios were calculated from the amounts of precursor salts used to prepare a particular catalyst. The theoretical and experimental bulk atomic ratios of Pt and Ru are the same, as neither the loss of Pt nor Ru was detected by UV/VIS spectroscopy. However, the UV/VIS spectroscopic studies showed that a considerable amount of tungsten (about 33 and 50% for the $PtWO_x$/C and $PtRuWO_x$/C catalyst, respectively) is lost as a result of the washing procedure. The loss of the tungsten component is believed to be due to dissolution of WO_x rather than due to unreacted $(NH_4)_6H_2W_{12}O_{40}$ precursor salt, as the use of an acidified washing solutions prevented the loss of tungsten entirely. Table 1 also shows the experimental atomic surface ratio of the catalysts obtained from XPS studies. The XPS data

Table 1. Theoretical and experimental atomic ratios* for carbon supported Pt based catalysts used in this work

Catalyst		Theoretical bulk atomic ratio†	Experimental bulk atomic ratio‡	Atomic surface ratio§
Pt/C	Pt	1	1	1
$PtWO_x$/C	Pt:WO_3	1:0.3	1:0.2	1:0.1
PtRu/C	Pt:Ru	1:0.85	1:0.85	1:2.7
$PtRuWO_x$/C	Pt:Ru:WO_3	1:0.85:0.3	1:0.85:0.15	1:2.5:0.17

Catalysts of Pt and Ru loadings of 32 and 16 wt % per carbon, respectively, were prepared.

* All atomic ratios are calculated using the sum of the non-carbon catalyst components (i.e., Pt, Ru and WO_x). For this calculation, the W component is assumed to be mainly in the (+VI) state (i.e., as WO_3) as supported by XPS studies.

† Theoretical bulk atomic ratios are calculated from the amount of precursor salts used for the preparation of a particular catalyst.

‡ Experimental bulk atomic ratios are obtained involving UV/VIS spectroscopic analysis of the washing solution of the catalysts, as described in the experimental section.

§ Atomic surface ratios are obtained from XPS studies of the as prepared catalyst powders.

suggest a higher Ru surface concentration in comparison to the bulk, that is, there is a surface enrichment of Ru for both the PtRu/C and $PtRuWO_x$/C catalyst powders. The Ru surface enrichment is seen to be significant, as the Ru surface atomic ratio is about 2.8 and 2.5 times higher than the bulk atomic ratio for the PtRu/C and $PtRuWO_x$/C catalyst, respectively. This surface enrichment of Ru may be caused by differences in the reaction rates of the individual precursor salts with the $NaBH_4$ solution, as in fact the reduction reaction of the Pt precursor is more rapid than the reduction reaction of the Ru precursor [12]. It should be noted that the Pt:WO_x ratio used here is equivalent to the ratio of the $PtWO_x$/C catalyst reported to be most active for the CH_3OH oxidation reaction by Shukla et al. [8]. The surface enrichment Ru suggests the catalyst particles to be nonuniform. Therefore, the surface ratios determined here by XPS analyses may not be accurate. The following sensitivity factors were used to calculate the atomic XPS ratios: 5.575 for Pt, 2.043 for Ru and 3.523 for W and mean free path values of 1.684 nm for Pt (4f), 1.536 nm for Ru (3p) and 1.757 nm for W (4f) were obtained using the electron effective attenuation length database version 1.0 from NIST.

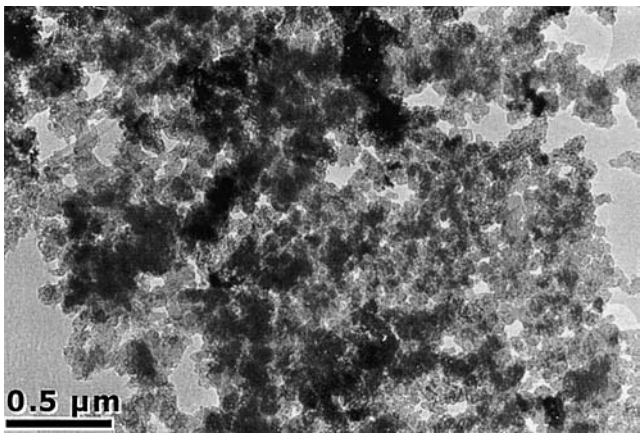

Fig. 1. TEM image at a 50 k magnification for the $PtRuWO_x$/C catalyst.

3.2. *TEM characterization*

Figures 1 and 2 show TEM images for the carbon supported catalysts prepared and studied in this work. Figure 1 shows a typical TEM image for the $PtRuWO_x$/C catalyst. At 50 k magnification, features of the carbon black powder are observed showing that agglomerates

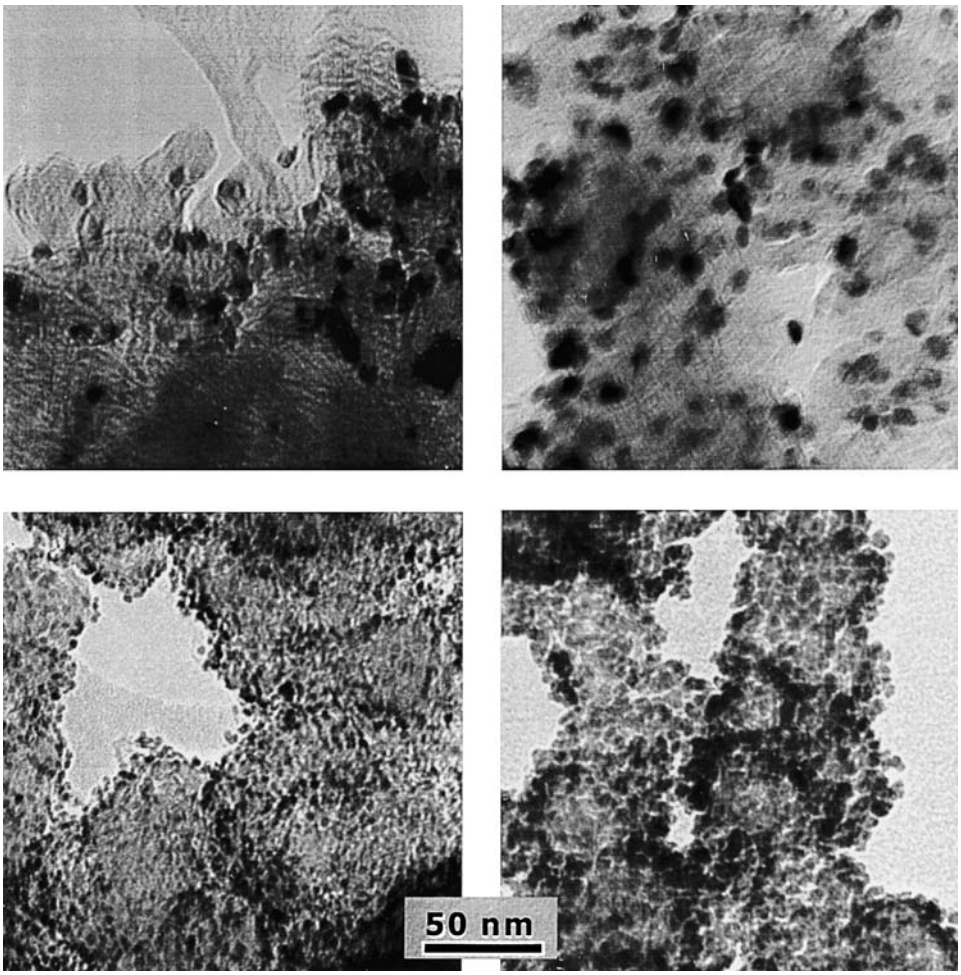

Fig. 2. TEM images at 400 k magnification for the catalysts of (a) Pt/C, (b) $PtWO_x$/C, (c) PtRu/C and (d) $PtRuWO_x$/C.

in the μm scale range are formed. The actual catalyst particles are recognizable in the higher magnification (400 k) images shown in Figure 2(a) to (d) for the four carbon supported catalyst powders. The higher resolution images show the catalyst particles to be in good physical, and hence, electrical contact with the carbon black support. The catalyst particles are seen to be in the nanoscale range. Their size depends on the catalyst composition and decreases in the following order: $PtWO_x$/C (6–15 nm) $\approx$ Pt/C (6–25 nm) > PtRu/C (2.5–5 nm). The particle size estimation for the $PtRuWO_x$/C catalyst from the TEM images is difficult, due to a large degree of particle agglomeration. The 'agglomerated' particles of the $PtRuWO_x$/C catalyst appear to form a network of loosely attached catalyst particles. A few, individual small catalyst particles in the size range similar to the PtRu/C catalyst (i.e., 2.5–5 nm) are observed for the $PtRuWO_x$/C catalyst. The TEM results suggest that the addition of Ru reduces the catalyst particle size (PtRu/C < Pt/C and $PtWO_x$/C), an influence that has been previously observed for carbon supported PtRu vs carbon supported Pt catalyst systems [13]. These influences on the catalyst particle size are expected to be beneficial in the case of the Ru addition, as the surface area per mass of catalyst increases upon Ru addition. It should be noted that a certain degree of particle agglomeration is observed for all catalysts. This results in an undesired decrease in the catalyst surface area available for the CH_3OH oxidation reaction. Furthermore, additional TEM images showed that catalyst coverage on the carbon black support to be nonuniform, that is, a significant number of carbon black particles were observed that were not covered with the actual catalyst particles.

3.3. *XRD characterization*

Figure 3 shows typical XRD spectra for the catalysts. The peak characteristics for the internal Si standard are clearly observed at 2θ of 28.44 (111), 47.30 (220), 56.12 (311), 69.13 (400), 76.38 (331) degrees [14]. Furthermore, the small and broad diffraction peaks at 25.9° observed in all spectra are attributed to the (002) plane of the hexagonal structure for carbon black. The platinum diffraction peaks for the (111), (200) and (220) phases are observed in the spectra of all catalysts. Diffraction peaks arising from crystalline tungsten oxide and Ru phases are not observed in the XRD spectra for any of these catalysts. The absence of diffraction peaks typical for 'crystalline' tungsten oxide could indicate that the WO_x is present in an amorphous form, as has been reported for $PtWO_x$/C catalysts prepared in the same manner as in this work [8]. The lack of the observation of Ru diffraction peaks can be partly assigned to the fact that some of the Ru is incorporated into the face centred cubic (f.c.c.) Pt lattice, as well as the fact that intensities of the Ru diffraction peaks are very weak. Figure 3(b) shows enlarged views of the Pt(111) diffraction peaks for the four catalysts studied in this work. It is seen that the

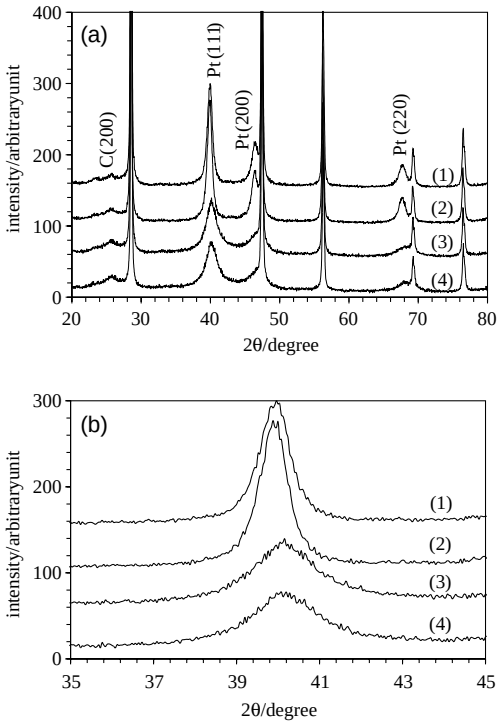

Fig. 3. XRD spectra for Pt/C (curve 1), $PtWO_x$/C (curve 2), PtRu/C (curve 3) and $PtRuWO_x$/C (curve 4) catalysts. Si was added as internal standard to the as prepared catalyst powders. Figure 3(a) shows scans between 20 and 60°, while Figure 3(b) shows the enlargement of the Pt(111) diffraction peaks between 35 and 45°.

Pt(111) diffraction peaks are shifted to higher 2θ values for the PtRu/C and the $PtRuWO_x$/C catalysts as compared to the Pt/C and $PtWO_x$/C catalysts. The following lattice parameter constants for f.c.c. Pt of 0.39(21) ($\pm$0.002), 0.39(22) ($\pm$0.003), 0.38(95) ($\pm$0.002) and 0.38(94) ($\pm$0.002) nm for Pt/C, $PtWO_x$/C, PtRu/C and $PtRuWO_x$/C catalysts, respectively, were estimated. It is well known that incorporation of Ru into the f.c.c. Pt lattice lowers the lattice constant in a linear fashion, that is, following Vegard's law [15]. The lattice parameter constants estimated for the PtRu/C and $PtRuWO_x$/C catalysts suggest that for both these catalyst powders, PtRu alloys of Pt to Ru atomic ratio of close to 0.75 to 0.25 are formed using the lattice parameter to PtRu ratio relationship estimated by Gasteiger et al. [16]. This atomic ratio estimated for the PtRu alloy phase indicates that not all of the Ru is incorporated into the f.c.c. Pt lattice, as this ratio is lower than the experimental bulk atomic Pt:Ru ratio (Table 1). This result suggests that a not alloyed Ru phase is present, which is often observed for supported PtRu catalysts. The high surface Ru concentration of the PtRu/C and $PtRuWO_x$/C catalysts (Table 1) may indicate that the not alloyed Ru is located at the surface of the catalyst particles. The Pt lattice parameter constants estimated for the Pt/C and $PtWO_x$/C catalyst powders are very similar to the lattice parameter constant value for pure f.c.c. Pt [17]. This indicates that tungsten (oxide) is not incorporated into the Pt lattice.

The average particle sizes for the Pt and PtRu alloy phases were also obtained using the Topas software program and the estimated values are listed in Table 2. According to the XRD data, the average particle size of the Pt and PtRu alloy phases decreases in the following order: $PtWO_x/C \approx Pt/C > PtRuWO_x/C \approx PtRuWO_x/C$. This average particle size estimation was carried out taking micro strain into consideration that was estimated to be relatively small, about 1%. These average particle sizes for the Pt and PtRu alloy phases are consistent with the particle size range observed for the Pt/C, $PtWO_x/C$ and PtRu/C catalysts by TEM.

The surface area (SA_{XRD}) of the Pt and PtRu alloy phases is roughly estimated, assuming homogeneously distributed and spherical particles, as follows:

$$SA_{XRD} = \frac{3}{r\rho_p} \quad (4)$$

In Equation 4, ρ_p is the density of either the Pt or PtRu alloy particle and r is the particle radius. The latter being assumed to be equivalent to one half of the average Pt and PtRu particle size estimated from the XRD data. Furthermore, the ρ_p values are calculated using the atomic percentages of Pt (at $\%_{Pt}$) and Ru (at $\%_{Ru}$) as well as the Pt (ρ_{Pt}) and Ru (ρ_{Ru}) densities of 21.4 and 12.2 g cm^{-3} [17], respectively, as follows:

$$\rho_p = \rho_{Pt} \times \text{at } \%_{Pt} + \rho_{Ru} \times \text{at } \%_{Ru} \quad (5)$$

The SA_{XRD} data shown in Table 2 are seen to be essentially the same for the Pt/C and $PtWO_x/C$ catalysts and very similar for the PtRu/C and $PtRuWO_x/C$ catalysts. These data will be compared to electroactive Pt + Ru surface areas estimated later in this work. It should again be noted that the calculation of these SA_{XRD} values is a rough estimation. Furthermore, the XRD data suggest the average Pt particles size for the Pt/C and $PtWO_x/C$ catalysts prepared in this work to be larger than for the catalysts prepared by Shukla et al. [8], who reported average Pt particle sizes of 6 and 6.7 nm for the as prepared Pt/C and $PtWO_x/C$ catalysts, respectively. These differences likely indicate some variations in the catalyst preparation procedures such as the rate of $NaBH_4$ addition [12] that influence particle size and surface concentrations.

3.4. *XPS characterization*

Figure 4(a)–(c) shows the XPS spectra for the Pt 4f, Ru 3p and W 4f core level regions collected for the $PtRuWO_x/C$ catalyst. The C 1s XPS peak (that results mainly from the carbon black support) superimposes with the intensive Ru 3d XPS peak. Therefore, both the less intensive, but single Ru 3p, as well as the Ru 3d XPS spectra are used to characterize the Ru component of the carbon supported catalysts studied here. Deconvolution of the C 1s spectra showed the majority of the carbon to be present in a peak located at 284.4 eV. The metallic Au 4f peak (84 eV) was used to estimate the C 1s binding energy. The position of the C 1s peak, that is, 284.4 eV was used to correct the binding energies for all catalysts for the small but observed charging effects. The spectra were deconvoluted using the peak half widths and area ratios for the spin orbit splitting peaks described in the literature [18–21]. The O 1s spectra of the different catalysts and the blank (untreated and catalyst free) carbon black support was also analysed suggesting the presence of —C=O groups (peak at 532.1 ± 0.15 eV) [18] and higher oxidized groups (538.6 ± 0.1 eV) on the carbon support. In the case of the Ru containing catalysts, an O 1s peak located at 529.9 ± 0.1 eV was also observed, which may suggest the presence of RuO_2 [19]; for the W containing catalysts, an O 1s peak at 530.7 eV was found that may suggest the presence of WO_3 [19, 20]. The presence of both RuO_2 and WO_3 in the corresponding catalysts was confirmed by the Ru 3p, Ru 3d and W 4f spectra, respectively, discussed below.

Table 3 summarizes the XPS results obtained by deconvoluting the Pt, Ru and W XPS spectra for all four carbon supported catalysts studied in this work. The deconvolution of the Pt 4f XPS spectra for all catalysts also suggests the presence of small amounts of possibly $PtCl_2$ in the presence of a Pt $4f_{7/2}$ peak located at 73.2 eV. This peak may reflect the fact that the Pt-

Table 2. Characteristics of the Pt and PtRu catalyst components: Average particle sizes and surface areas

	Pt /C	$PtWO_x$ /C	PtRu /C	$PtRuWO_x$ /C
XRD particle size*/nm	13.9	14.3	4.6	4.6
$SA_{XRD}/m^2\ g^{-1}_{(Pt\ or\ PtRu\ alloy)}$ †	20	22	68	68
$SA_{(Pt+Ru)}/m^2\ g^{-1}_{(Pt\ +\ Ru)}$ ‡	16.1	15.7	31	41
$\frac{SA_{(Pt+Ru)}}{SA_{XRD}}$	0.8	0.7	0.5	0.6

* Average particle size values calculated from the peak half width of the Pt XRD diffraction peaks using Topas 2 software program. Values are estimated with an error of ±3%.

† Pt + Ru surface areas (SA_{XRD}) estimated from the corresponding average particle size values listed in row 2 using Equation 2. As noted, in the text these numbers represent rough estimates.

‡ Electroactive Pt + Ru surface areas ($SA_{(Pt+Ru)}$) calculated from the CO stripping charge Q_{COads} using a charge to Pt + Ru surface area conversion factor of 420 $\mu C\ cm^{-2}$, as discussed in the text. Reproducibility of the CO adsorption method is within ±10%.

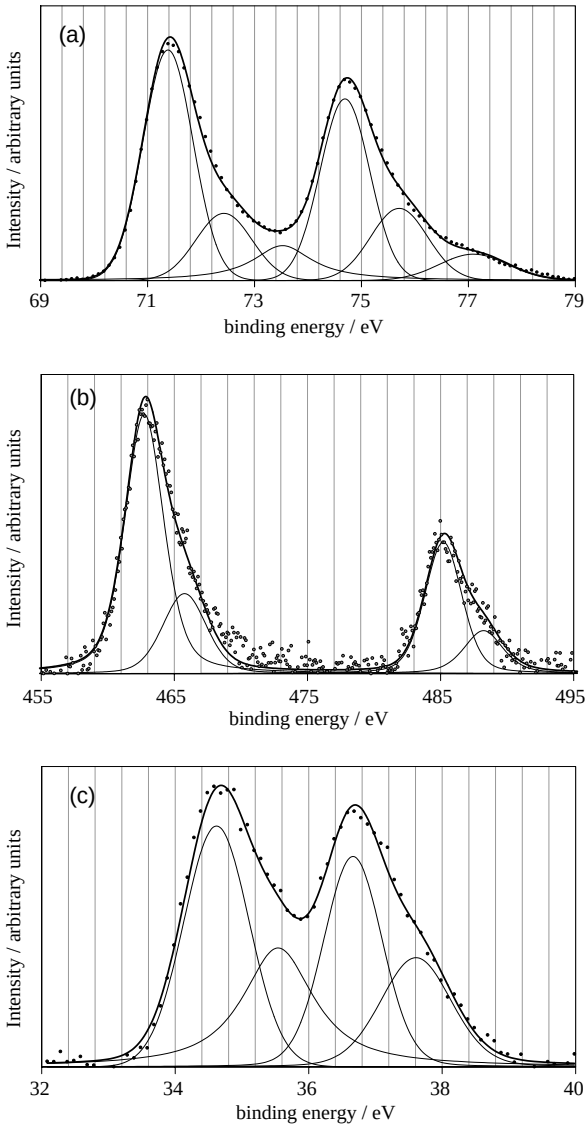

Fig. 4. Typical XPS spectra for the Pt 4f (a), Ru 3p (b) and W 4f (c) regions. The XPS spectra were obtained for the as prepared $PtRuWO_x/C$ catalyst. The dotted points represent the experimental data. Thin lines show the deconvolution results; the individual peaks obtained using computer fitting of the experimental data and the thick line shows the complete curve fit (i.e., the sum of the deconvoluted curves). The C 1s peak (284.4 eV) was used to correct all XPS spectra. The metallic Au 4f peak (84 eV) was used to estimate the C 1s binding energy.

chloride precursor salt is not completely reduced and trace amounts of chloride remain on the catalysts, as in fact small Cl peaks were observed in the survey spectra for all catalysts at about 198 eV. Table 3 shows that the XPS data suggest the surface Pt to be mainly present as Pt metal (about 70–80 at %), indicated in a Pt $4f_{7/2}$ peak located at 71.2 ± 0.1 eV, and PtO (about 30–20 at %), indicated by a Pt $4f_{7/2}$ peak located at 72.2 ± 0.1 eV. These results suggest that the majority of the Pt surface sites are present in easily reducible forms, as needed for CH_3OH oxidation catalysts as shown in Reaction 1.

The XPS results for the Ru 3p spectra (Table 3 and Figure 4(b)) suggest that the Ru surface species consist of a mainly (about 80 at %) Ru component in a lower oxidation state, viewed as an intermediate between Ru metal and Ru(+IV)-oxide, as similarly reported by Arico et al. [18]. The position of this XPS Ru $3p_{3/2}$ peak component is located at 462.8 eV. The XPS data also suggest the presence of a small (about 20% of the surface Ru) amount of RuO_2 in a Ru $3p_{3/2}$ peak located at 466.5 eV for the two Ru containing catalysts [19]. The Ru 3d XPS spectra confirmed the presence of both the lower Ru component (intermediate between Ru metal and Ru(+IV)-oxide) and RuO_2 in $3d_{5/2}$ peaks located at about 280.3 and 281.4 eV, respectively [19]. Furthermore, the XPS data suggest the amount and type of surface Ru to be the same for the PtRu/C and $PtRuWO_x/C$ catalyst. The W 4f XPS spectrum for the $PtWO_x/C$ catalyst indicates the presence of WO_3 in a peak at 35.5 eV (for W $4f_{7/2}$), while the W 4f spectrum for the $PtRuWO_x/C$ catalysts suggests the presence of mainly (about 80 at %) WO_3 and a more reduced (about 20 at %) W(+V)-oxide in the presence of W $4f_{7/2}$ peaks at 35.4 and 34.6 eV, respectively [19, 20]. These XPS results suggest that the tungsten is present in the form of a mixed (+V) and (+VI) tungsten oxide, and hence, is referred to as WO_x (value of x between 2.5 and 3).

Overall, it can be said that the XRD and XPS results suggest that the WO_x does not influence the electronic (chemical) properties of the Pt, Ru and/or PtRu components of the catalysts prepared in this work that use single metal precursor salts for the catalyst synthesis. This is consistent with extended X-ray absorption fine structure (EXAFS) studies carried out for catalysts systems prepared using single metal salt precursors and bimetallic precursor salts [22]. Pt–W interactions were only observed for the catalysts prepared using the bimetallic precursor salt. Furthermore, the XRD data suggest that the average Pt and PtRu particle size, that is, the average particle size of key catalyst components, are not influenced by the addition of tungsten. The real surface area as well as accessibility of the fuel to the active sites, however, may be influenced by the tungsten addition, as partly indicated by the TEM studies and further discussed below using CO_{ads} studies.

3.5. *CO_{ads} stripping voltammetry*

Prior to the electrochemical CH_3OH oxidation studies, the catalysts and a polycrystalline Pt foil were characterized using CO_{ads} stripping voltammetry shown in Figures 5 and 6. In these figures, the thick line shows the CO_{ads} stripping voltammogram, that is, the first cycle recorded after the adsorption of CO, while the thin line shows the second cycle that is equivalent to the background CV of the catalyst under study. The background CVs for the Pt foil, Pt/C and $PtWO_x/C$ catalyst electrodes (Figure 5(a)–(c)) show the well-known H adsorption/desorption peaks ($H_{ads/des}$) that are characteristic of polycrystalline Pt and the typical Pt-oxide formation and reduction features are also

Table 3. Binding energies and atomic surface concentrations of different species from curve fitted XPS spectra for the carbon supported catalysts

Catalyst	Species	Binding energy /eV	Assignment	Concentration /at %*
Pt/C	Pt $4f_{7/2}$	71.2	Pt metal	76
		72.1	PtO	24
$PtWO_x$/C	Pt $4f_{7/2}$	71.2	Pt metal	73
		72.1	PtO	27
	W $4f_{7/2}$	34.6	W(+V)-oxide	64
		35.5	WO_3	36
PtRu/C	Pt $4f_{7/2}$	71.3	Pt metal	80
		72.5	PtO	20
	Ru $3p_{3/2}$	462.8	Intermediate between Ru(0) and (+IV)	77
		466.5	RuO_2	23
$PtRuWO_x$/C	Pt $4f_{7/2}$	71.4	Pt metal	69
		72.1	PtO	31
	Ru $3p_{3/2}$	462.8	Intermediate between Ru(0) and (+IV)	77
		466.5	RuO_2	23
	W $4f_{7/2}$	34.6	W(+V)-oxide	78
		35.4	WO_3	22

Note: The C 1s peak (284.4 eV) was used to correct for possible charging effects. The metallic Au 4f peak (84 eV) was used to calibrate the C 1s peak.

* Atomic surface concentration (at %) of the components of a particular element estimated from the ratio of the area of the deconvoluted peaks of the XPS spectra of the element of interest.

observed [23]. The background CV characteristics for the PtRu/C and $PtRuWO_x$/C catalysts are dominated by the redox characteristics typical for Ru that overlay with the $H_{ads/des}$ Pt CV characteristics shown in Figure 6(a) and (b), consistent with previous studies [4]. The CO_{ads} stripping voltammograms observed for the Pt foil, Pt/C and $PtWO_x$/C catalyst electrodes (Figure 5(a)–(c)) generally show a small prewave between about 0.2–0.6 V and the main CO_{ads} stripping peak(s) at higher potentials. The prewave is likely due to the oxidation of weakly adsorbed CO, while the more positive stripping peak reflects the presence of strongly adsorbed CO [24]. Prewaves have been previously observed for polycrystalline Pt electrodes and are known to depend on the potential employed to adsorb CO. In some cases, seen here for the Pt and $PtWO_x$/C catalysts, the main stripping peak is split into more than two peaks. This has also been observed in previous work and could indicate the presence of different surface states of the catalysts [26]. In fact, up to three CO_{ads} stripping peaks are observed for Pt catalysts in the nanoscale range, a behaviour, which has been assigned to different facets of nanosized vs bulk Pt [27]. It is also seen that the oxidation of the adsorbed CO takes place at lower potentials for the Ru containing catalysts consistent with literature data indicating the capability of Ru containing Pt based catalysts to oxidize adsorbed CO at lower potentials.

For a 1 cm^2 geometrical area polycrystalline Pt foil electrode, hydrogen desorption charge (Q_{Hdes}) and CO_{ads} stripping charge (Q_{COads}) values of 194 and 391 μC, respectively, were found. These Q_{Hdes} and Q_{COads} values suggest Pt areas of 0.9 cm^2 and 0.93 cm^2, respectively using charge to area conversion factors of 210 $\mu C\ cm^{-2}$ for the one electron H_{des} reaction and 420 $\mu C\ cm^{-2}$ for the two electron CO_{ads} to CO_2 oxidation reaction. The fact that very similar Pt areas are obtained using the experimentally observed H_{des} and CO_{ads} charge values suggests that close to one monolayer of CO is adsorbed under the experimental conditions used here. The CO_{ads} charge can also yield a measurement for the electroactive Pt + Ru area [26]. It is known that CO adsorbs on Pt and metallic Ru sites [26], while its adsorptive interactions with oxide covered surfaces such as WO_x are generally small. Therefore, the Q_{COads} values yield measurements of the Pt area for the Pt/C and $PtWO_x$/C catalysts, while the Q_{COads} values yield estimates of the Pt + Ru surface area for the PtRu/C and $PtRuWO_x$/C catalysts. It should be noted that the contribution of Ru to the CO_{ads} surface area measurements arises from Ru sites that are in the reduced form at the potential where CO is adsorbed [27]. The position of the CO_{ads} stripping peak for the PtRu/C and $PtRuWO_x$/C catalysts is somewhat lower than for the corresponding bulk PtRu alloy catalysts [25]. This difference is believed to be related to the fact that in this work catalyst particles in the nanoscale range are used. Furthermore, the unalloyed Ru phase could also distort the CO_{ads} stripping voltammogram characteristics.

Table 2 summarizes the noble metal surface areas ($SA_{(Pt + Ru)}$) obtained from the experimentally observed CO_{ads} charges, that is, using a charge to area conversion factor of 420 $\mu C\ cm^{-2}$. The CO_{ads} method suggests an increase in the Pt + Ru electroactive surface areas in the following order: $PtWO_x/C \approx Pt/C < PtRu/C < PtRuWO_x/C$. In fact, the CO_{ads} and the area estimation using the average Pt and PtRu alloy particle size obtained from the XRD data are very similar for the Pt/C and $PtWO_x$/C catalysts. However, the Pt + Ru surface areas estimated using the CO_{ads} method are

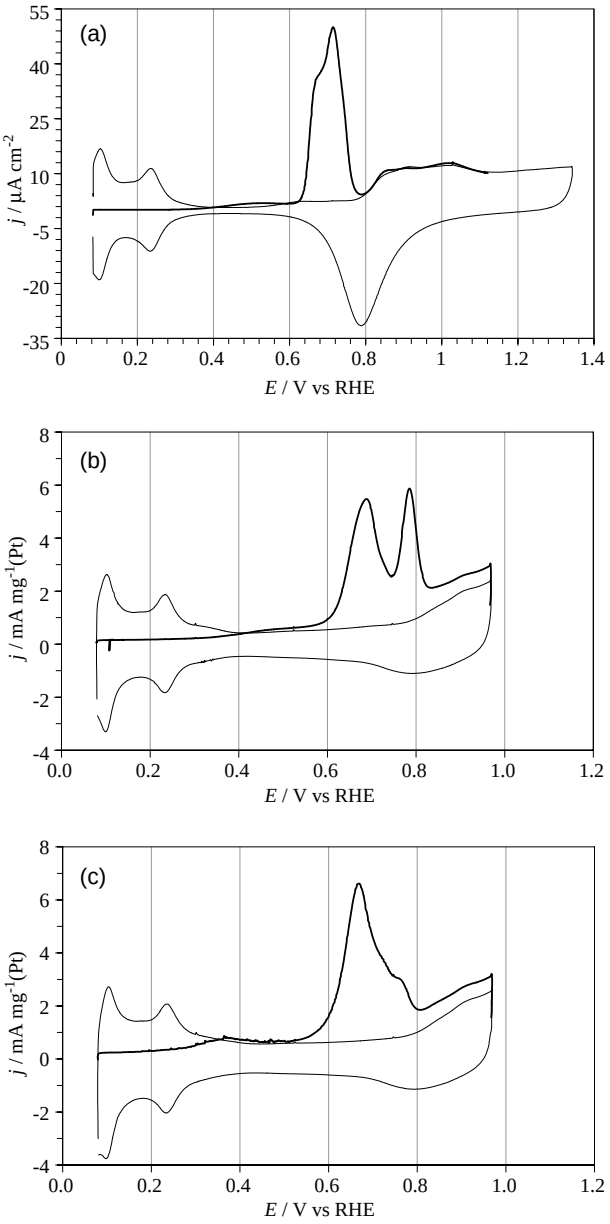

Fig. 5. CO_{ads} stripping voltammograms recorded at 10 mV s^{-1} in 0.5 M H_2SO_4 for a polycrystalline Pt foil electrode (a), the Pt/C catalysts (b) and the $PtWO_x$/C catalysts (c). Solid line shows the first cycle i.e., (the CO_{ads} stripping peak), while the thin line shows the second cycle (i.e., the background CV of the electrode in 0.5 M H_2SO_4). In the case of the Pt foil electrode (a), the current scale is normalized by the geometrical electrode area, while the current scales for the Pt/C and $PtWO_x$/C catalysts (b) and (c) are normalized for the mass of Pt used for the electrochemical measurements.

significantly smaller (about 50%) than the surface area estimated using the average particle size. This difference may be explained by the presence of, for example, WO_x and RuO_2 species on the catalyst particle surface that are thought to be inactive towards the adsorption reaction of CO and may block access of CO to the PtRu alloy surface sites. Furthermore, surface area values calculated using the average Pt and PtRu alloy particle sizes, that is, the SA_{XRD} values, need to be used with caution as they are likely to have a very significant error.

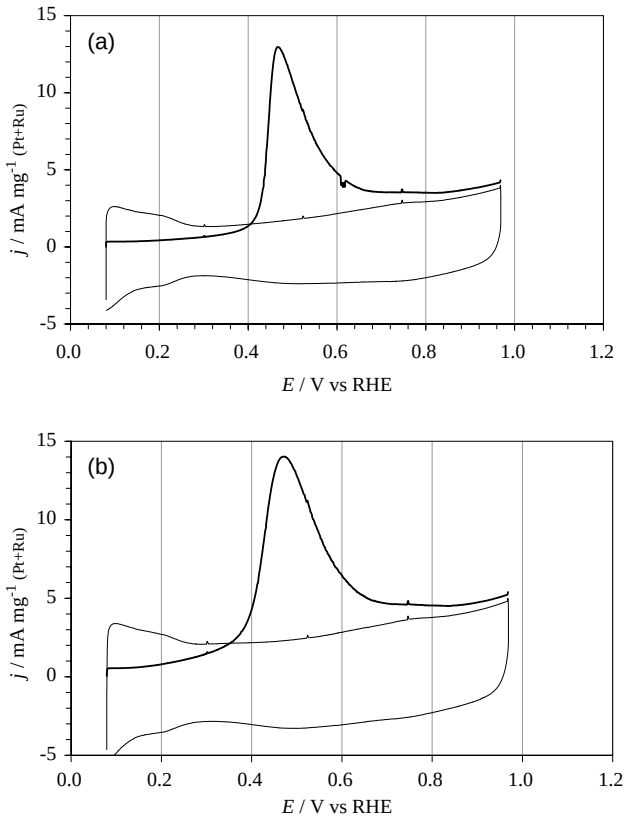

Fig. 6. CO_{ads} stripping voltammograms recorded at 10 mV s^{-1} in 0.5 M H_2SO_4 for the PtRu/C catalysts (a) and the $PtRuWO_x$/C catalysts (b). Solid line shows the first cycle (i.e., the CO_{ads} stripping peak) while the thin line shows the second cycle (i.e., the background CV of the electrode in 0.5 M H_2SO_4). Current scales are normalized for the mass of Pt + Ru used for the electrochemical measurements.

3.6. *CH_3OH oxidation studies*

In this Section, the CH_3OH oxidation activities for the powder catalyst electrodes was determined from slow sweep CVs and potential–time transients recorded at constant current densities. All CH_3OH oxidation experiments were carried out at 60 °C using 1 M CH_3OH + 0.5 M H_2SO_4 solutions. First, slow sweep CV data obtained between 0.07 and 0.9 V at 1 mV s^{-1} are discussed. The CV studies were carried out using a series of repetitive experiments as follows: First, three complete oxidation/reduction cycles at 10 mV s^{-1} were recorded, followed by two complete cycles at 1 mV s^{-1}. This 'cycling procedure' was repeated a total of three times. Steady-state CV curves were obtained for both the first and second cycle recorded at 1 mV s^{-1} and the CV data were essentially the same for all three experiments. The monitored currents were normalized for the noble metal mass, $m_{Pt + Ru}$, and the $SA_{(Pt + Ru)}$ values, and are hence referred to as $j_{mass(Pt + Ru)}$ and $j_{SA(Pt + Ru)}$, respectively. Figure 7 shows the CH_3OH oxidation data for the Pt/C and $PtWO_x$/C catalysts, while Figure 8 shows the same, but for the PtRu/C and $PtRuWO_x$/C catalysts. Furthermore, Figures 7(a) and 8(a) show the $j_{mass(Pt + Ru)}$ against E curves, while Figures 7(b) and 8(b) show the $j_{SA(Pt + Ru)}$ against E

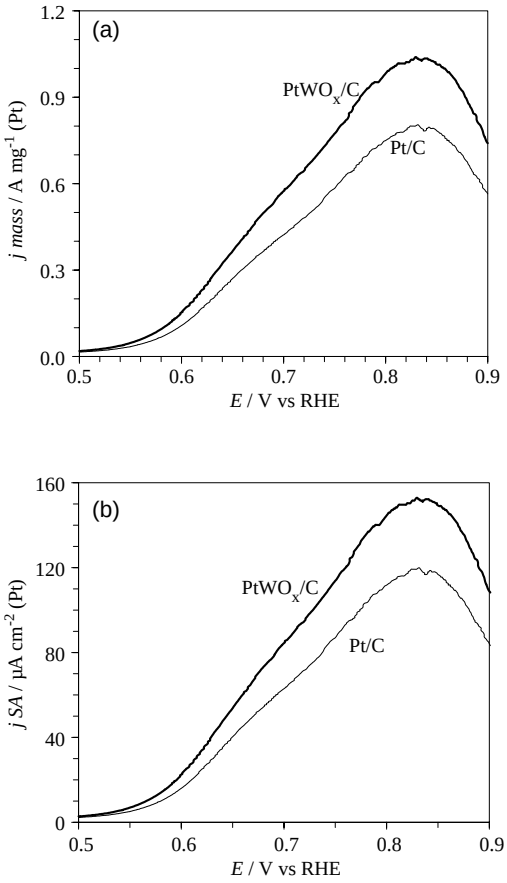

Fig. 7. Slow sweep CVs recorded at 1 mV s^{-1} in 1 M CH_3OH + 0.5 M H_2SO_4 at 60 °C for the Pt/C and $PtWO_x$/C catalysts. Current scale is normalized for the Pt mass (a) and for the Pt area estimated from CO_{ads} experiments (b).

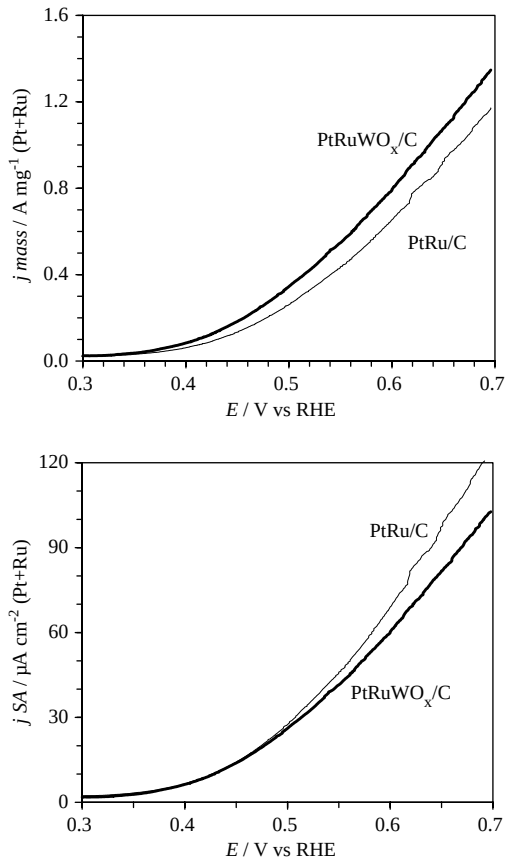

Fig. 8. Slow sweep CVs recorded at 1 mV s^{-1} in 1 M CH_3OH + 0.5 M H_2SO_4 at 60 °C for the PtRu/C and $PtRuWO_x$/C catalysts. Current scale is normalized for the Pt + Ru mass (a) and for the Pt + Ru area estimated from CO_{ads} experiments (b).

curves. For both sets of catalysts, Pt/C vs $PtWO_x$/C and PtRu/C vs $PtRuWO_x$/C, the WO_x containing catalyst appear to yield slightly higher mass normalized currents. However, the shape and onset oxidation potential for a particular set of catalysts, Pt/C vs $PtWO_x$/C and PtRu/C vs $PtRuWO_x$/C, are essentially the same. In fact, the dynamic Tafel slope values estimated from these slow sweep CVs are essentially the same for a particular set of catalysts, about 60 mV per current decade for Pt/C and $PtWO_x$/C and about 90 mV per current decade for PtRu/C and $PtRuWO_x$/C catalysts. These results suggest that the WO_x component of the catalysts studied here does not exhibit a true catalytic effect (e.g., a bifunctional influence) towards the CH_3OH oxidation reaction. In fact, normalizing the monitored current by the electro-active surface area of Pt + Ru for the PtRu/C and $PtRuWO_x$/C catalysts (i.e., $j_{SA(Pt + Ru)}$ vs E curves shown in Figure 8(b)) results in essentially identical curves. This clearly indicates that the small improved performance per Pt + Ru weight for the $PtRuWO_x$/C vs the PtRu/C catalyst is not due to a true catalytic effect of WO_x towards the CH_3OH oxidation reaction. The surface area normalized CV curves for the Pt/C and $PtWO_x$/C catalysts (Figure 7(b)) suggest a somewhat improved performance (about 30% higher mass normalized currents) for the $PtWO_x$/C than the Pt/C catalyst. However, it should be noted that the value of this small increase is close to the error (of ±10% per catalyst) of the Pt surface area estimated using the CO adsorption method.

Figure 9(a) and (b) show the potential–time (E/t) transients as a function of the current normalized by the noble metal mass ($j_{mass(Pt + Ru)}$) and the Pt + Ru area ($j_{SA(Pt + Ru)}$), respectively. The E values were recorded after 5 min at a constant current value for the four catalysts studied in this work. Pseudo steady-state E/t transients were obtained within the first seconds at a particular current value. The potential values obtained in this manner are estimated with ±15% error. The applied current values were maintained small (0.05–6.5 mA) to avoid large amounts of H_2 formation at the cathode that may depolarize the anode potential. It is seen that the CH_3OH oxidation activity for particular $j_{mass(Pt + Ru)}$ and $j_{SA(Pt + Ru)}$ values increases in the order: Pt/C < $PtWO_x$/C < PtRu/C < $PtRuWO_x$/C over a broad potential range. In fact, almost constant potential differences are observed between the different catalysts for the tested range of $j_{mass(Pt + Ru)}$ values, for example, PtRu/C ~0.05 V, $PtWO_x$/C ~0.155 V and Pt/C ~0.18 V more positive than $PtRuWO_x$/C. The potential differ-

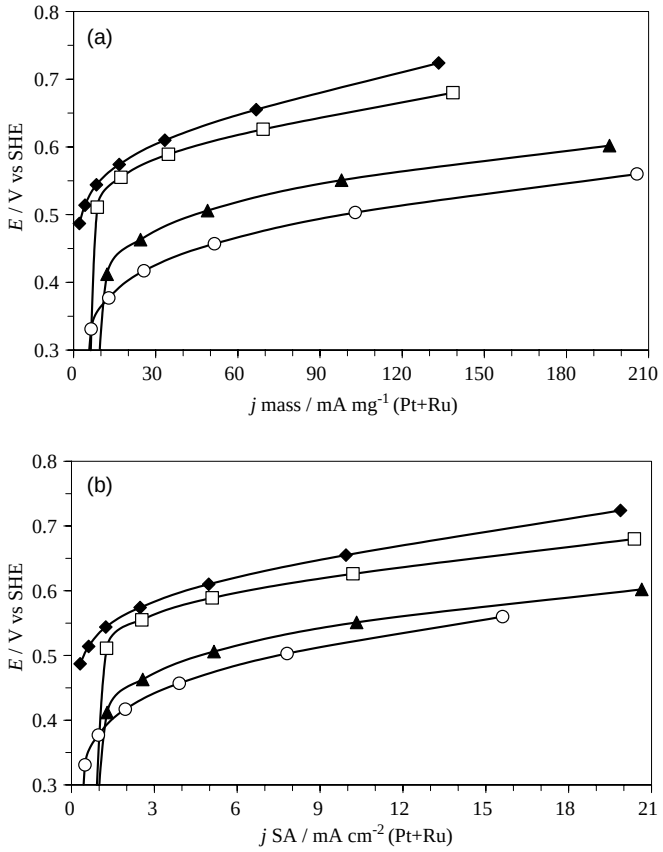

Fig. 9. Potential (E) against current density (i) plots for the Pt/C (♦), $PtWO_x$/C (□), PtRu/C (▲) and $PtRuWO_x$/C (○) catalysts. Pseudo steady-state potential values were obtained after 5 min at a particular, constant current in 1 M CH_3OH + 0.5 M H_2SO_4 at 60 °C. Applied current values were normalized by the Pt + Ru mass (a) and the noble metal surface area estimated from CO_{ads} experiments (b). Solid lines present the computer best fit to the experimental data.

ences obtained at a particular $j_{SA(Pt + Ru)}$ value show a similar trend, namely, PtRu/C ~0.03 V, $PtWO_x$/C ~0.125 V and Pt/C ~0.14 V more positive than PtRu-WO_x/C. The potential differences observed for the surface area normalized curves, that is, the E against $j_{SA(Pt + Ru)}$ graphs, are less pronounced for a particular set of catalysts, namely 0.015 V for the Pt/C vs the $PtWO_x$/C catalysts and 0.03 V for the PtRu/C vs $PtRuWO_x$/C catalysts than found for the mass normalized curves, consistent with the CV results. The error in these potential difference measurements that result from errors in the potential measurement and errors in the electroactive Pt + Ru surface area estimations are relatively high, that is, close to the small potential differences observed for a particular set of catalysts. Therefore, the experimental $E/j_{SA(Pt + Ru)}$ and $E/j_{mass(Pt + Ru)}$ curves probably indicate that the WO_x components of the catalysts studied here do not exhibit a true catalytic effect, consistent with the CV data. However, in the case of PtRu/C and $PtRuWO_x$/C catalysts, the WO_x component appears to have a beneficial influence on the PtRu surface area accessible for CH_3OH.

It should be noted that the potential differences for the mass normalized current curves for the Pt/C and $PtWO_x$/C catalysts observed here (~0.025 V) are significantly smaller than the potential differences of 0.15 V reported by Shukla et al. [8]. They, however, obtained this 0.15 V difference by extrapolating their data to a high current load of 0.8 A cm^{-2} geometrical area (equivalent to applied current load of 0.64 A per mg Pt) and high anode potentials of about 0.75 and 0.9 V. Estimation of the potential difference for their Pt/C and $PtWO_x$/C catalysts (for which they reported different Tafel slope values) in the similar current per Pt mass density range studied here shows that their difference is of a similar order of magnitude as observed here (e.g., at 0.15 A per mg Pt the data reported by Shukla et al. indicate a 0.03 V difference for the Pt/C vs the $PtWO_x$/C catalysts). However, the experimentally monitored potential values at a particular constant current per Pt weight value are significantly higher (almost 0.15 V) for the Pt/C and $PtWO_x$/C catalysts studied in this work as compared to the data reported by Shukla et al. [8]. This difference likely indicates that Shukla et al. [8] prepared catalysts of higher surface area to Pt mass catalysts ratios than done in this work, consistent with their and our particle size estimation. It is also noteworthy that the $j_{mass(Pt + Ru)}$ values found in this work for the PtRu/C catalysts are smaller (by about two times) than for more optimized (i.e., smaller PtRu nanoparticles) while they compare to other data obtained for larger PtRu

particles [28]. This shows the strong influence of the particle size on the $j_{mass(Pt + Ru)}$ values.

4. Summary and conclusions

High surface area Pt/C, $PtWO_x$/C, PtRu/C and $PtRuWO_x$/C catalysts have been prepared using a simple impregnation and subsequent chemical reduction route commonly used for the preparation of fuel cell catalysts. XPS studies indicated that the tungsten oxide of the 'as-prepared' catalysts is present in the VI+ or V+ oxidation state, that is, with an x value varying between 2.5 and 3. No evidence was found that the tungsten influences the electronic properties of the Pt and Ru catalyst components. XRD studies showed Ru to be partly incorporated into the fcc Pt lattice forming a PtRu alloy of Pt:Ru atomic ratios of about 0.75:0.25 independent of the presence of WO_x. The addition of Ru was clearly seen to decrease the average catalyst particle size, consistent with a higher electroactive Pt + Ru surface areas estimated from CO_{ads} stripping voltammetric charges. In the case of the Ru containing catalysts, the addition of the WO_x component appears to result in a porous network of agglomeration, however only loosely attached catalyst particles. Pt + Ru surface area values estimated using the CO_{ads} method suggest that the electroactive Pt + Ru surface area for the $PtRuWO_x$/C catalyst to be somewhat (~25%) larger than for the PtRu/C catalyst.

CH_3OH oxidation activities were obtained from slow sweep CV experiments as well as potential–time transients obtained at constant currents for all four catalysts. The electrodes consisted of thin catalyst layers that were prepared at low temperature and the preparation method avoided the use of a hot press, thus minimizing alterations of catalyst properties. The experimentally obtained CH_3OH oxidation activities per Pt + Ru weight indicated some differences, while the CH_3OH oxidation activities per Pt + Ru surface area were very similar for a particular set of catalysts, that is, Pt/C vs $PtWO_x$/C and PtRu/C vs $PtRuWO_x$/C. The latter suggests that WO_x does not exhibit a true catalytic activity for the CH_3OH oxidation reaction for the catalysts studied in this work. This is consistent with the i/V shape (dynamic Tafel slopes) and CH_3OH onset potential obtained from the slow sweep CV studies that were essentially identical for the Pt/C vs $PtWO_x$/C and PtRu/C vs the $PtRuWO_x$/C catalysts. Therefore, observed differences in CH_3OH oxidation activities per Pt + Ru weight are assigned to 'physical' changes in catalyst properties such as electroactive Pt + Ru surface area.

It should be emphasized that CV studies do not provide ultimate information of catalyst performance under real fuel cell operating conditions. However, CV studies yield measurements about the activity, as well as the chemistry, of the process/catalysts under study. In the case for CH_3OH oxidation catalysts, they provide an essential understanding of the true catalytic activity of the anode catalyst tested.

Acknowledgements

The authors thank D. Wang and G. Pleizier (National Research Council Canada) for the TEM and XPS analyses, respectively as well as P. L'Abbe (National Research Council Canada) for the preparation of the electrochemical glass cells used in this work.

References

1. W. Vielstich, 'Fuel Cells' (John Wiley & Sons, New York, 1970).
2. K. Scott, W.M. Taama and P. Argyropoulos. *J. Power Sources* **79** (1999) 43.
3. J. O'M. Bockris and H. Wroblowa, *J. Electroanal. Chem.* **7** (1964) 428.
4. M. Watanabe and S. Motoo, *J. Electroanal. Chem.* **60** (1975) 267.
5. A. Haner and P.N. Ross, *J. Phys. Chem.* **95** (1991) 3740.
6. B. Gurau, R. Viswanathan, R. Liu, T.J. Lafrenz, K.L. Ley, E.S. Smotkin, E. Reddington, A. Sapienza, B.C. Chan, T.E. Mallouk and S. Sarangapani, *J. Phys. Chem. B* **102** (1998) 9997.
7. P.K. Shen and A.C.C. Tseung, *J. Electrochem. Soc.* **141** (1994) 3082.
8. A.K. Shukla, M.K. Ravikumar, A.S. Arico, G. Candiano, V. Antonucci, N. Giordano and A. Hamnett, *J. Appl. Electrochem.* **25** (1995) 528.
9. M. Gotz and H. Wendt, *Electrochim. Acta* **43** (1998) 3637.
10. T.D. Jarvi and E.M. Stuve, *in* J. Lipkowski and P.N. Ross (Eds), 'Electrocatalysis' (Wiley–VCH, New York, 1998), p. 139.
11. A.J. Bard and L.R. Faulkner, 'Electrochemical Methods, Fundamentals and Applications' (John Wiley & Sons, New York, 1980).
12. C. Bock, B. MacDougall and Y. LePage, *J. Electrochem. Soc.*, Submitted.
13. E. Antolini, L. Giorgi, F. Cardellini and E. Passalacqua, *J. Solid State Electrochem.* **5** (2001) 131.
14. Scintag, Inc., 'X-ray Diffraction database' (Diffraction Management System for Windows NT, Scintag Inc., Cupertina, CA, 1997).
15. B.E. Warren, 'X-ray Diffraction' (Dover Publications, New York, 1990).
16. H.A. Gasteiger, P.N. Ross, Jr., and E.J. Cairns, *Surf. Sci.* **293** (1993) 67.
17. D.R. Lide, 'CRC Handbook of Chemistry and Physics' (CRC Press, Boston, 71st edn, 1990–1991).
18. A.S. Arico, P. Creti, P.L. Antonucci, J. Cho, H. Kim and V. Antonucci, *Electrochim. Acta* **43** (1998) 3719.
19. C.D. Wagner, 'Handbook of X-ray Photoelectron Spectroscopy' (Perkin–Elmer Corp., Physical Electronics Division, 1979).
20. P. Biloen and G.T. Pott, *J. Catal.* **30** (1973) 169.
21. G.M. Bancroft, I. Adams, L.L. Coatsworth, C.D. Bennewitz, J.D. Brown and W.D. Westwood, *Anal. Chem.* **47** (1975) 586.
22. O.S. Alexeev, G.W. Graham, M. Shelef and B.C. Gates, *J. Catal.* **190** (2000) 157.
23. B.E. Conway, H. Angerstein-Kozlowska, W.B.A. Sharp and E. Criddle, *Anal. Chem.* **45** (1973) 1331.
24. F. Richarza, B. Wohlmanna, U. Vogela, H. Hoffschulza and K. Wandelt, *Surf. Sci.* **335** (1995) 361.
25. H. Gasteiger, N. Markovic, P. Ross and E. Cairns, *J. Phys. Chem.* **98** (1994) 617.
26. K.A. Friedrich, F. Henglein, U. Stimming and W. Unkauf, *Electrochim. Acta* **45** (2000) 3283.
27. C. Bock and B. MacDougall, *J. Electrochem. Soc.* **150** (2003) 377.
28. T.J. Schmidt, H.A. Gasteiger and R.J. Behm, *Electrochem. Com.* **1** (1999) 1.